Peng *et al*. *Complex Eng Syst* 2024;4:15
**DOI:** 10.20517/ces.2024.08

Complex Engineering Systems

Research Article

Open Access

# Multiple unmanned aerial vehicle collaborated three-dimensional electromagnetic target situation map construction

**Yuqing Peng[1], Kun Liu[1], Xuezhao Cai[1], Jie Wang[1], Zhipeng Lin[1]**

[1]College of Electronic and Information Engineering, Nanjing University of Aeronautics and Astronautics, Nanjing 211106, Jiangsu, China.

**Correspondence to:** Dr. Zhipeng Lin, College of Electronic and Information Engineering, Nanjing University of Aeronautics and Astronautics, 29 Jiangjun Road, Jiangning District, Nanjing 211106, Jiangsu, China. E-mail: linlzp@nuaa.edu.cn; ORCID: 0000-0001-5941-2163

**How to cite this article:** Peng Y, Liu K, Cai X, Wang J, Lin Z. Multiple unmanned aerial vehicle collaborated three-dimensional electromagnetic target situation map construction. *Complex Eng Syst* 2024;4:15. http://dx.doi.org/10.20517/ces.2024.08

**Received:** 21 Feb 2024 **First Decision:** 6 Jun 2024 **Revised:** 9 Jul 2024 **Accepted:** 22 Jul 2024 **Published:** 26 Jul 2024

**Academic Editor:** Hamid Reza Karimi **Copy Editor:** Fangling Lan **Production Editor:** Fangling Lan

## Abstract

The electromagnetic (EM) target situation map can visualize the situation and locations of multiple EM targets in the three-dimensional (3D) space. It is vital for the spectrum activity monitoring, radiation source localization, frequency resource management, and so on. Traditional studies focused on the radio environment map construction, and the characteristics such as locations of EM targets are not accurate due to reconstruction deviation and environmental noise. This paper presents a 3D EM target situation map construction scheme based on multiple unmanned aerial vehicle collaboration. Firstly, an improved maximum and minimum distance clustering-based algorithm is proposed to estimate the number and rough location of EM targets directly by utilizing the original sparse sampling data. Then, to improve the accuracy of situational awareness, a re-weighted map fusion algorithm is used to update the raw EM characteristics results. Finally, we calculate the self-information of different targets and optimize the previous location results. Compared with other conventional methods, numerical results demonstrate that the proposed method has higher mapping accuracy under the same low sampling rate.

**Keywords:** Multi-UAV collaboration, 3D electromagnetic target situation map, clustering algorithm, re-weighted fusion

## 1. INTRODUCTION

With the rapid development of wireless communication, plenty of radio, mobile phones, navigation and other equipment and systems have been integrated into the electromagnetic (EM) network, resulting in an increasingly complex EM environment[1–4]. The spatial distribution of EM targets is one of the important characteristic pieces of information in EM space. An electromagnetic target situation map (ETSM) can quantitatively characterize and visualize the quantity, position, power, and other information of EM targets[5]. It effectively solves the monitoring and locating of multiple EM targets in complex scenarios.

Take the traditional radio environment map (REM) as an example, whose composition process is also known as spectrum mapping. The construction process of REM accounts for the variations in the spatial distribution of EM environments in practical applications, making a realistic description of the EM environment possible. A complete REM construction system can achieve the perception, reconstruction, storage, and visualization of EM environment information[6]. The REM system is primarily composed of four main modules: measurement capable devices (MCDs), prior information database, cognitive engine, and storage and retrieval unit[7]. Depending on the type of platform used in MCDs, the REM mapping systems can be divided into three categories: space-based, ground-based, and air-based. Among these, space-based mapping systems, such as Kleos Space in France and HawkEye360 in the United States, use artificial satellites to gather global spectrum information. Researches on ground-based mapping systems are more mature currently, most of which use handheld spectrum analyzers, spectrum monitoring vehicles, and spectrum sensing sensors arranged in interested areas to obtain ground spectrum information. The German unmanned aerial vehicle (UAV) monitoring system Colibrex LS OBSERVER AMU is a typical air-based mapping system; however, the measurement range is extremely limited due to its tethered structure. Du *et al.* proposed an aerial spectrum situational mapping system based on UAV platform, which can achieve the construction of air-ground spectrum situational maps[8–10].

The restoration of EM environment based on sparse sampling spectrum data, i.e., map completion, is the key component of the above system. The completion methods for REMs can be classified into two categories: data-driven and model-driven[11]. Data-driven methods mainly include spatial interpolation algorithms, matrix (tensor) completion algorithms, and machine learning-based methods. Inverse distance weighted (IDW)[12], also known as Shepard method, is a classic spatial interpolation technique with fast completing speed and high smoothness. To solve the problem of completing multidimensional spectrum data, tensor-based completion methods are proposed[13]. Hashimoto *et al.* propose a spatial interpolation with convolutional neural networks (SICNN) method based on deep learning[14]. Above all, these data-driven methods can directly estimate the spectrum data of unsampled positions without any prior knowledge, but usually require a large amount of observation spectrum data and with lower accuracy. The models in model-driven methods mainly refer to the propagation loss (PL) model of wireless channels. Classic model-driven methods contain active transmitter location estimation-based method (LIvE)[15], Received Signal Strength Difference (RSSD)-based method[16], *etc*. However, both LIvE and RSSD assume that there is only one EM target in the monitored area, which cannot solve the spectrum completion problem in complex environments. Compared with data-driven methods, model-driven methods usually have superior completion accuracy; however, they require prior information such as the position, number of EM targets, and the precise channel propagation model[17–19]. In recent years, multi-channel spectrum sensing studies based on deep learning neural networks have begun to emerge, but such methods are overly dependent on datasets and often ignore the actual EM propagation rules[20–22].

In order to obtain precise information about EM targets, it is necessary to address the localization problem of EM targets[23]. At present, source-free positioning methods represented by Direction of Arrival (DOA) and Time Difference of Arrival (TDOA) have been applied in various studies[24,25]. However, these methods require multiple antenna signal receiving devices and have high hardware costs. Thus, single antenna localization methods based on Received Signal Strength (RSS) have been paid much more attention in recent years.

Liu *et al.* used an UAV system equipped with a single antenna to collect data and achieved rapid localization in urban scenes based on RSS method[26]. On the other hand, due to the correlation and similarity between spectrum data, clustering methods such as K-means, DBSCAN (Density-Based Spatial Clustering of Applications with Noise), Gaussian Mixture Model (GMM), *etc.* are widely used in RSS-based localization[27]. With the development of deep learning, neural network structure is introduced into clustering algorithms. Aiming to solve the problem of large-scale high-dimensional spectrum data that are difficult to handle through traditional clustering methods, a semi-supervised K-means algorithm is proposed[28]. However, the above clustering methods did not consider the propagation characteristics of EM waves, making it difficult to accurately classify spectrum data and obtain the position of EM targets.

Overall, the main contributions of this paper are summarized as follows:

• An EM target awareness system based on collaborative multiple UAVs (multi-UAVs) is designed for collecting spectrum data, which solves the issue of sampling errors that are prone to occur in complex environments or at high altitudes. And a mathematical model of the three-dimensional (3D) ETSM combined with actual EM propagation rules is constructed.

• A map fusion algorithm based on re-weighting is proposed. The algorithm enhances the reconstruction results of data-driven method by modeling the fusing process as a least absolute shrinkage and selection operator (LASSO) regression problem.

• An improved maximum and minimum distance (MMD)-based EM target staged-location method is proposed. By optimizing the characteristic parameter of MMD with a proper PL model, the rough positions of EM targets can be fast derived based on raw spectrum data. The ultimate location result is modified with fused spectrum data.

The rest of this paper is organized as follows. Section 2 gives the composition of the collaborative multi-UAV system and the 3D ETSM model. In Section 3, the details of the proposed 3D ETSM construction scheme are given and demonstrated. Simulation results and analysis are provided in Section 4. Finally, we make a summary and conclusion in Section 5.

## 2. SYSTEM MODEL

### 2.1. Collaborative multi-UAV system

In recent years, UAVs have been widely used in various communication systems due to their advantages of high maneuverability, low risk, and low cost. However, it is challenging to build lightweight systems because of load and storage capacity limits. The proposed hardware EM target awareness system is shown in Figure 1. It consists of three parts: autonomous control of UAVs, aerial spectrum measurement, and fuse-construction of EM target situation. The details of each part are as follows.

The UAV platform subsystem includes a Global Positioning System (GPS) receiving module, an integrated communication and remote control module, a flight control module, and an image module. Via information exchanges through the integrated communication and remote control module, the GPS receiving module receives GPS position information obtained from the ground. The flight control module controls the flight of UAVs. The image module transmits the collected images to the ground processing terminal. Note that an UAV platform subsystem is equipped with a spectrum measurement subsystem.

The spectrum measurement subsystem includes a spectrum receiver, measurement antenna, and microcomputer. It is responsible for collecting and analyzing spectrum information.

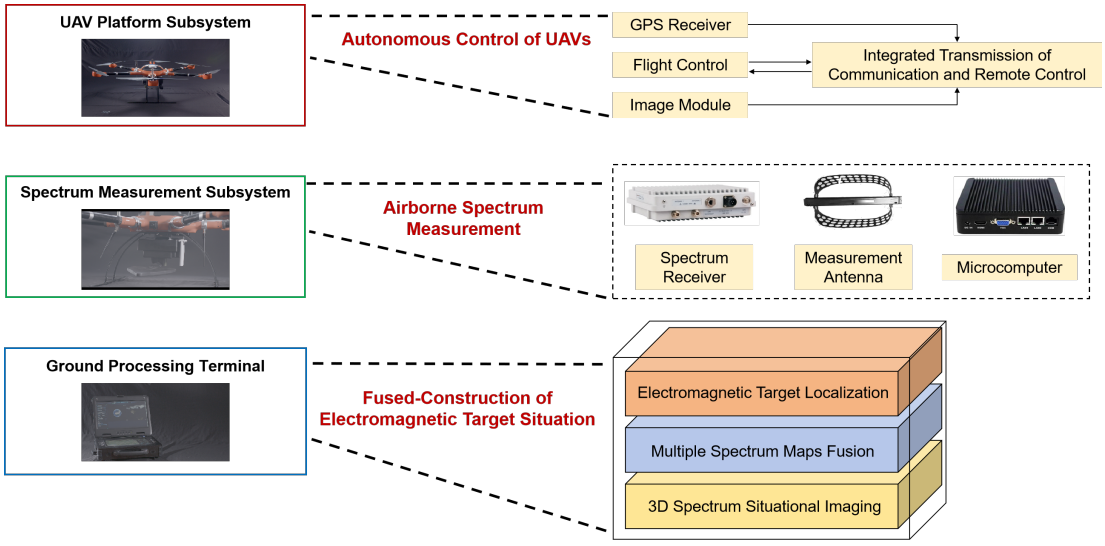


**Figure 1.** UAV-assisted system of EM target awareness.

The ground processing terminal sends the information gathered from the integrated communication and remote transmission module to the ground station. The ground station is equipped with a software platform to integrate, process, analyze the sampling data, and construct the 3D ETSM of the interested area.

### 2.2. 3D ETSM model

In this paper, multi-UAVs loaded spectrum measurement modules are used to obtain the initial spectrum data, and the collaborative sampling model is shown in Figure 2. In order to simplify the data volume to be processed in the following steps, the monitored area is divided into $N = N_x \times N_y \times N_z$ cubes, and each cube is numbered as $(n_x, n_y, n_z)$. Assuming that the grid scale of the cubes is $m$, ETSM of the entire area can be modeled as a third-order tensor $\boldsymbol{\varphi} \in \mathbb{R}^{N_x \times N_y \times N_z}$.Then, in a 3D Cartesian coordinate system, center point of each cube can be expressed as

$$S(x, y, z) = ((n_x - 0.5) \times m, (n_y - 0.5) \times m, (n_z - 0.5) \times m). \tag{1}$$

According to the distribution of obstacles, the ground terminal sends GPS information through the integrated communication and remote control module for route planning of UAVs. Each UAV conducts uniform sparse sampling of spectrum data along the pre-set trajectory respectively, i.e., RSS values are observed at $R$ positions, which can be expressed as a transposed matrix $\boldsymbol{\varphi} = [\varphi_1, ..., \varphi_R]^{\mathrm{T}}$. Assume that the number of UAVs is $G$, and the number of sampling points for the $g$-th UAV is $R_g$. The sampling rate of the ETSM system can be defined as

$$SR_{\text{aver}} = \frac{1}{G} \sum_{g=1}^{G} (R_g / N). \tag{2}$$

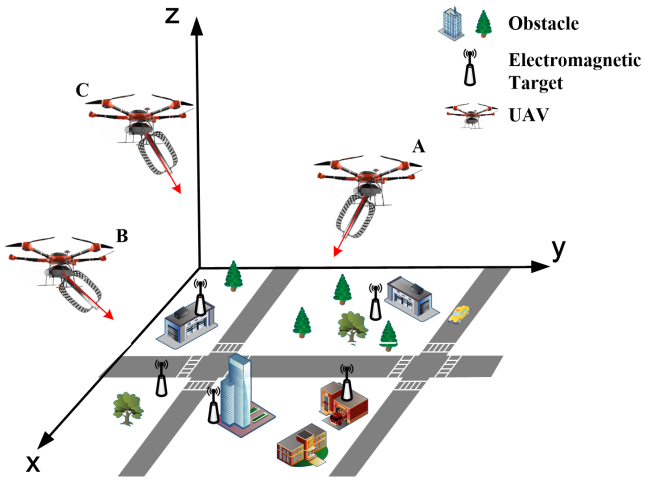


**Figure 2.** Multi-UAV collaborative sampling model.

## 3. 3D ETSM CONSTRUCTION WITH MULTI-UAV COLLECTED DATA

The construction scheme of 3D ETSM is shown in Figure 3. We first propose an improved MMD-based clustering algorithm to obtain a preliminary estimate of target positions. Then, we design a map fusion algorithm to reconstruct the fused spectrum map. Finally, we modify the preliminary estimation of target positions and obtain the precise positions.

### 3.1. MMD-based electromagnetic target rough location

An improved MMD-based clustering algorithm is proposed in this section for the approximate localization of EM targets. MMD is a pattern recognition probing-based clustering technique, which is based on Euclidean distance and takes objects as far as possible as the cluster center. Therefore, compared with K-means method, it prevents the chance of cluster centers being too close to each other when selecting initial values[17]. In addition to finding the number of the initial clustering centers rapidly, this method can increase the efficiency of spectrum data partition.

The basic MMD algorithm first starts with a sample object as the first cluster center, then selects a sample that is the farthest from the first cluster center as the second cluster center. Afterwards, other cluster centers are determined based on the maximum distance in succession, until no new cluster centers are generated. Finally, classify the samples into the nearest class according to the principle of minimum distance, and the division of the dataset is completed. However, in actual scenarios, the RSS value may be affected by the transmission distance, reflection, refraction, diffraction, and dispersion of EM waves during propagation, *etc.*[29]. Additionally, the attenuation of EM wave strength during transmission varies greatly with distance. The basic MMD method only considers the distance factor to cluster RSS data within the monitored area and cannot locate EM targets.

To accomplish the estimation of the EM target position within the monitored area, we improve the MMD algorithm by the PL rules in this paper. Given that the 3D ETSM of the monitored area contains $N$ cubes, we consider the average RSS value within each cube representing a region as the RSS value at the center of that cube, denoted as $P_n(x_n, y_n, z_n)$, $n = 1, 2, ..., N$. Since the prior knowledge of EM targets is unknown, we take the total sampling spectrum data of multi-UAVs as the input dataset, and select an arbitrary sampling cube $S_i(x_i, y_i, z_i)$, $i = 1, 2, ..., R'$ as the first clustering center $Z_1(x_1, y_1, z_1)$, where $R'$ is the total number of sampling points corresponding to the multi-UAV system. To ensure that the next selected cluster center has a higher

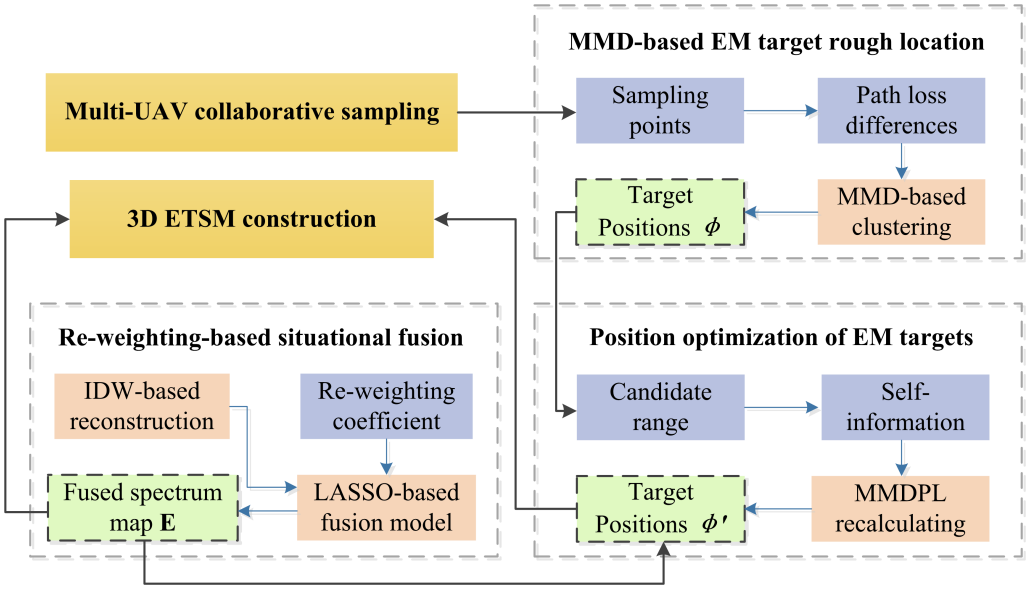


**Figure 3.** Overview of 3D ETSM construction.

possibility of being the location of the EM target, the path loss difference calculation is chosen to replace the distance calculation in the clustering algorithm. Path loss between the $k$-th clustering center and the $i$-th cube can be expressed as

$$\Delta\hat{P}_{ki} = \left|\Delta P_{ki} - L_i\right|, \quad k < N, \tag{3}$$

where

$$\Delta P_{ki} = \left|P_k - P_i\right|, \tag{4}$$

which denotes the difference of RSS between the $k$-th clustering center and the $i$-th cube. $L_i$ is the path loss of EM wave strength in free space, which can be calculated as

$$L_i(\mathrm{dB}) = 32.45 + 20\lg(f) + 20\lg(d_{ki}), \tag{5}$$

$$d_{ki} = \sqrt{(x_{Z_i} - x_i)^2 + (y_{Z_i} - y_i)^2 + (z_{Z_i} - z_i)^2}, \tag{6}$$

where $f$ is the frequency of EM targets, $d_{ki}$ is the Euclidean distance between the $k$-th clustering center and the $i$-th cube. Next, calculate the path loss from all other sampling points to $Z_1$, if

$$\Delta\hat{P}_{k1} > \max_i\{\Delta\hat{P}_{i1}\}, \tag{7}$$

**Algorithm 1: MMPLD**

Input: iteration counter k=0, sampled data $\mathbf{P}$.
Output: EM target positions $\boldsymbol{\phi} = [\phi_1, ..., \phi_K]^{\mathrm{T}}$
Initialization: set of clustering centers $\mathbf{Z} = \emptyset$
Randomly select an arbitrary sampling point from $\boldsymbol{S}$ as the first clustering center $Z_1$ and add it to $\mathbf{Z}$.
For $k = 1$ to the desired number of EM targets, do:
  a. Initialize the maximum path loss difference $\max_i\{\Delta\hat{P}_{i1}\} = 0$
  b. For each sampling point $S_i$ in $\boldsymbol{S}$, do:
    i. If $S_i$ is not assigned to any cluster center yet, then:
      - Calculate the path loss difference $P_{ki}$ between $S_i$ and all cluster centers in $\mathbf{Z}$ by Equation (7)
    ii. If $\Delta\hat{P}_{k1} > \max_i\{\Delta\hat{P}_{i1}\}$, then:
      - Update $\max_i\{\Delta\hat{P}_{i1}\} = \Delta\hat{P}_{k1}$
      - Set the current sampling point $S_i$ as the next cluster center candidate
  c. Add the next cluster center candidate to $\mathbf{Z}$
  d. Assign all sampling points in $\boldsymbol{S}$ to the nearest cluster center based on the path loss difference
Return $\boldsymbol{\phi} = [\phi_1, ..., \phi_K]^{\mathrm{T}}$

then, $S_k$ is taken as the second clustering center $Z_2$. Then, the $(k+1)$-th clustering center can be determined by

$$\begin{aligned} & Z_{k+1} = Z_j, \\ s.t. \quad & \Delta\hat{P}_{pj} = \max\{\min(\Delta\hat{P}_{1i}, \Delta\hat{P}_{2i}, ..., \Delta\hat{P}_{ki})\}, \\ & (p = 1, 2, ..., k), \end{aligned} \tag{8}$$

where $\Delta\hat{P}_{ki}$ denotes the path loss from the $k$-th clustering center to the $i$-th cube. For fast convergence, when $\Delta\hat{P}_{pj} \leq \theta \cdot \Delta\hat{P}_{12}$, the calculating process ends, where $\Delta\hat{P}_{12}$ is the path loss from $Z_1$ to $Z_2$. $\theta$ is a clustering parameter that determines the number of clusters, usually determined by probing. All sampling points are divided based on the differences of path losses according to K-Nearest Neighbor (KNN) principle, and the clustering centers are considered as EM targets; i.e., the rough position estimation result $\boldsymbol{\phi} = [\phi_1, ..., \phi_K]^{\mathrm{T}}$ of EM targets is obtained. In this case, the improved MMD algorithm is recalled as Maximum Minimum Propagation Loss Difference (MMPLD) method. Algorithm 1 summarizes the process of MMD-based EM target rough location.

### 3.2. Re-weighting-based situational fusion

In this section, we design a map fusion algorithm based on re-weighting to enhance the accuracy of spectrum data, which can significantly improve the accuracy of ETSM construction and further localization of EM targets.

#### *3.2.1 spectrum reconstruction based on IDW*

Since the sampling data are sparsely distributed in the monitored area, we first get the initial spectrum maps corresponding to each single-UAV by IDW.

Classic IDW method assumes that the influence of the sampling value of a known point on the estimated value of an unknown point depends on the distance between the sampling point and the unknown point. To obtain the RSS value $\hat{P}_{S_0}$ of the unknown cube $S_0$, the weight coefficient $\omega_n$ is calculated by using the weighted average of RSS data $P_{S_n}, n = 1, 2, ..., N$ of its nearest $N$ known cubes $S_n$, which can be expressed as

$$\omega_n = \frac{d_n^p}{\sum_{i=1}^{N} d_i^p}, \tag{9}$$

where $d_n$ is the distance between $S_0$ and $S_n$, parameter $p$ controls the decrease rate of the weight coefficient $\omega_n$ with distance, which usually taken as -2. The IDW method is called inverse distance squared weighting method at this time. Thus, the RSS value of the unknown point $S_0$ can be calculated by

$$P_0(x_0, y_0, z_0) = \sum_{n=1}^{N} \omega_n P_n(x_n, y_n, z_n). \tag{10}$$

Traditional IDW method only considers the effect of distance, ignoring the influences of other factors (*e.g.*, frequency) on the RSS in actual EM propagation environment. In order to improve the performance of the traditional IDW, the weight coefficient can be improved based on the PL model as

$$\omega_n = \frac{\left(10 \lg\left(\frac{4\pi f d_n}{c}\right)\right)^{-2}}{\sum_{n=1}^{N}\left(10 \lg\left(\frac{4\pi f d_n}{c}\right)^{-2}\right)}, \tag{11}$$

where $f$ is the frequency of the received signal, $c$ is the speed of light, and $d_n = \sqrt{(x_0 - x_n)^2 + (y_0 - y_n)^2 + (z_0 - z_n)^2}$ is the Euclidean distance from the $n$-th sampling point $(x_n, y_n, z_n)$ to the interpolated point $(x_0, y_0, z_0)$. Define $\chi_n$ as the tensor of the 3D ETSM and assign the RSS value of the sampled point $P_i$ and the RSS value of the unknown point $P_n$ obtained by IDW inference to the map tensor $\chi_n$. Then, calculating Equations (10) and (11), multiple independent spectrum maps based on sparse sampling of single-UAVs are completed for the next fusion processing.

*3.2.2 Fusion model based on LASSO regression*

In order to reduce the limitation of the information provided by single-UAVs, a LASSO regression fusion model is proposed to process the above initial maps.

We define the initial maps corresponding to $G$ UAVs as $(\mathbf{M}_1, \mathbf{M}_2, ...\mathbf{M}_G)$, and the map obtained by the $g$-th UAV can be vectorized as spectrum data to be fused as $\mathbf{m}_g \in \mathbb{R}^N$. The fused data are defined as $\boldsymbol{\varepsilon}_g \in \mathbb{R}^N$, which are initialized to zero vectors. By applying the $\ell_1$ - norm to describe the spatial correlation degree of the fused data, the LASSO regression problem can be expressed as

$$\arg\min_{\boldsymbol{\varepsilon}_g}\left(\sum_{g}^{G}\left(\mathbf{m}_g - \mathbf{I}_N\boldsymbol{\varepsilon}_g\right)^2 + \tau\left\|\boldsymbol{\varepsilon}_g\right\|_1\right), \tag{12}$$

where $\mathbf{I}_N$ is the identity matrix, $\tau$ is the penalty coefficient, $\left\|\boldsymbol{\varepsilon}_g\right\|_1$ can be calculated as

$$\left\|\boldsymbol{\varepsilon}_g\right\|_1 = \sum_{g}^{G}\left|\boldsymbol{\varepsilon}_g\right|. \tag{13}$$

Combined with the EM propagation model, when the targets are observed with different strengths, the performance of Equation (13) can be enhanced by exploiting another weighting function. Large weights are used

to discourage nonzero entries, while small weights are used to encourage zero entries. Then, the weighting function $\mathbf{v}_N$ can be expressed as

$$\mathbf{v}_N^{(i)} = \begin{cases} \left( \sum_g^G \left( \boldsymbol{\varepsilon}_g^{(i-1)} \right)^2 \right)^{-1/2}, & \text{if } \left\| \boldsymbol{\varepsilon}_g \right\|_1 > 0, \\ 1/\rho, & \text{if } \left\| \boldsymbol{\varepsilon}_g \right\|_1 = 0, \end{cases} \tag{14}$$

where $\mathbf{v}_N^{(i)}$ denotes the re-weighting coefficient for the $i$-th iteration, and $\rho$ is a constant slightly greater than zero. By introducing the re-weighting term $\mathbf{v}_N$ in Equation (14), the optimization problem proposed in Equation (12) can be rewritten as a re-weighting fusion model as

$$\arg\min_{\boldsymbol{\varepsilon}_g} \left( \sum_g^G \left( \mathbf{m}_g - \mathbf{I}_N \boldsymbol{\varepsilon}_g \right)^2 + \mathbf{v}_N \cdot \tau \left\| \boldsymbol{\varepsilon}_g \right\|_1 \right), \tag{15}$$

which can be solved by Least Angle Regression (LARS)[30]. Finally, we can obtain the ultimate fused spectrum situation map $\mathbf{E}$ by

$$\mathbf{E} = \text{ivec} \left( \frac{1}{G} \sum_g^G \boldsymbol{\varepsilon}_g \right), \tag{16}$$

where ivec( · ) is the inverse of vectorization. By calculating Equation (16), the fused RSS data $\boldsymbol{\varphi}$ for position optimization can be obtained.

### 3.3. Position optimization of electromagnetic targets

In this section, the localization results in Section 3.1 are modified based on the fused map data. Since the number of EM targets is $K$, taking the $k$-th estimated target as an example, we extend a distance of the total length outward by 10% along the x-axis, y-axis and z-axis, respectively. We use this range as a candidate range $\Upsilon_k$. The sampled data $\boldsymbol{\upsilon}_k = [\upsilon_{k_1}, ..., \upsilon_{k_n}]^{\mathrm{T}} \in \mathbb{C}^{N_k}$ contained in the range $\Upsilon_k$ is used to locate the accurate position of the EM target in that range. $\upsilon_{k_n}$ corresponding to $\phi_{i_n}$ satisfies

$$\begin{aligned} \phi_{i_x} - 0.1 \cdot L_x \le \varphi_{k_{nx}} \le \phi_{i_x} + 0.1 \cdot L_x, \\ \phi_{i_y} - 0.1 \cdot L_y \le \varphi_{k_{ny}} \le \phi_{i_y} + 0.1 \cdot L_y, \\ \phi_{i_z} - 0.1 \cdot L_z \le \varphi_{k_{nz}} \le \phi_{i_z} + 0.1 \cdot L_z, \end{aligned} \tag{17}$$

Taking the central point of a certain $\phi_k$ cube as the origin point, we first extend a distance of the total length outward by 10% along the x-axis, y-axis and z-axis, respectively. Then, we get a correction range for $\phi_k$.

If there are other candidate targets within the range, the completed data within the range need to be corrected by

$$\hat{\upsilon}_{k_n} = \upsilon_{k_n} - \frac{\lambda^2}{\left( 4\pi \cdot d \left( \phi_i', \varphi_{k_n} \right) \right)^2}, \tag{18}$$

where $\phi_i'$ is the location of other candidate targets within the range, $\varphi_{k_n}$ is the location of the cube to be modified in the range that corresponds to $\phi_i$, and $\upsilon_{k_n}$ is the fused data at a certain grid.

Next, the amount of self-information can be measured by calculating the entropy in the range for measuring[31],

$$\boldsymbol{\upsilon}_k = \left[\left\lfloor 10\lg \widehat{\upsilon}_{k_1} \right\rfloor, \left\lfloor 10\lg \widehat{\upsilon}_{k_2} \right\rfloor, \ \ldots, \left\lfloor 10\lg \widehat{\upsilon}_{k_n} \right\rfloor\right]^{\mathrm{T}}. \tag{19}$$

We take the fused data of the grids at the top 70% of the information entropy as the effective sampling data for correcting the position of the EM targets. The localization results can be updated by recalculating Equation (8); i.e., initial positioning result $\boldsymbol{\phi} = [\phi_1, \ldots, \phi_K]^{\mathrm{T}}$ is modified to $\boldsymbol{\phi'} = \left[\phi_1', \ldots, \phi_K'\right]^{\mathrm{T}}$. Finally, the EM target localization is annotated on the fused map, and the ultimate 3D ETSM is constructed.

## 4. SIMULATION RESULTS AND ANALYSIS

In this section, the performance of the proposed 3D ETSM construction method is analyzed and verified under the campus scenario. The satellite map of the monitored area is shown in Figure 4. To validate the performance of the proposed method in complex environments while maintaining clarity, we only show the simulation results of the example region (ER). The ER includes various environmental factors such as grass, trees, and buildings that affect signal propagation. This allows us to verify the performance of the proposed method in complex environments. Moreover, the smaller range of the area helps to display the results more clearly. Assuming that the ER is 100 m × 100 m × 50 m. The 3D area is divided into 10 × 10 × 10 cubes, and each cube is 10 m × 10 m × 5 m. We utilize Radio Frequency (RF) transmitters to simulate EM targets. We can choose any frequency of interest to obtain the 3D ETSM at that frequency. Since many wireless devices currently operate in the 2.4 GHz band, we set the working frequency of each signal RF transmitter as 2.4 GHz. The other simulation parameters are shown in Table 1, where the positions of the RF transmitters are randomly selected. In other words, EM targets may be placed in various locations such as grasslands, roads, indoors, rooftops, *etc*. The transmitting power of different RF transmitters can be set arbitrarily. To more clearly display the simulation results, we set the transmitter power as 30 dBm in the simulation. The numbers of RF transmitters and UAVs in ETSM construction performance can also be set arbitrarily. Considering the limitations of existing equipment for future measurements, we set them to 5 and 3, respectively.

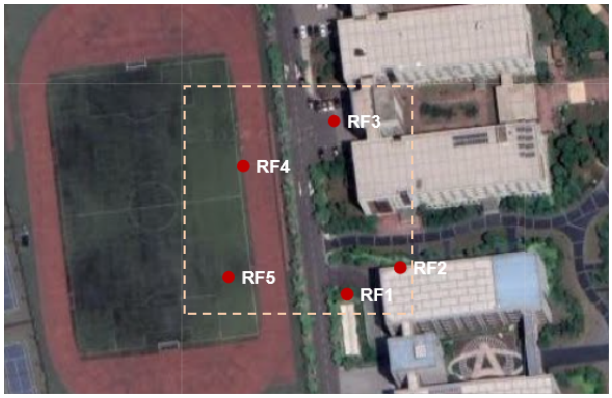


**Figure 4.** 3D ETSM construction scenario.

**Table 1. The main simulation parameters**

| Parameters | Value |
|---|---|
| The monitored area | 100 m × 100 m × 50 m |
| ETSM tensor size | 10 × 10 × 10 |
| Granularity of ETSM tensor | 10 m × 10 m × 5 m |
| Number of RF transmitters ($\kappa$) | 5, 7, 9, 11 |
| Transmitting power | 30 dBm |
| Transmitting frequency ($f$) | 2.4 GHz |
| Sampling rate, number of RF transmitters, and number of UAVs in ETSM construction performance | $SR_{\text{aver}} = 0.1, K = 5, G = 3$ |
| The heights of UAVs | 5 m, 10 m, 20 m |
| Positions of RF transmitters (x, y, z) | (91 m, 68 m, 13.9 m), (79 m, 293.5 m, 47 m), (236.5 m, 127.5 m, 34.6 m), (327.5 m, 423.5 m, 18.7 m), (459 m, 166.5 m, 3 m) |

As shown in Figure 5 (left), the ideal ETSM is calculated by Ray Tracing (RT) method. Assuming that three UAVs sample the ideal map along different paths, with the sampling rate of each UAV set to 10%, an original spectrum map obtained by a random single-UAV is shown in Figure 5 (middle). The ultimate 3D ETSM constructed by our method is shown in Figure 5 (right). As shown in Figure 5, one single-UAV system cannot accurately recover the ETSM, especially when the distance between two adjacent EM targets is too close. The performance of the ultimate ETSM is superior to that of the single-UAV system. This is because we fuse the observation data from multi-UAVs and eliminate outliers. When using the observation data from a single-UAV to construct the map, the presence of outliers in the data affects the accuracy of map construction.

Next, taking a two-dimensional plane at a certain height in the 3D ETSM as an example, the process and performance of the staged EM target positioning method are demonstrated in Figure 6. Firstly, we set three EM targets at the same XoY plane, which is re-divided into 50 × 50 grids, and size of each grid is 2 m × 2 m. The ideal map of the XoY plane is shown in Figure 6 (left). Then, maintain the sampling rate as 10%, rough positions based on raw data are shown in Figure 6 (middle), and the ultimate result is shown in Figure 6 (right). The red spiders denote the estimated positions of EM targets. Results show that the accuracy of the estimated EM target positions based on MMPLD can be improved by the fused ETSM, which effectively reduces mistakes in the first step of localization. This is because the RSS values used for localization become more accurate after fusion.

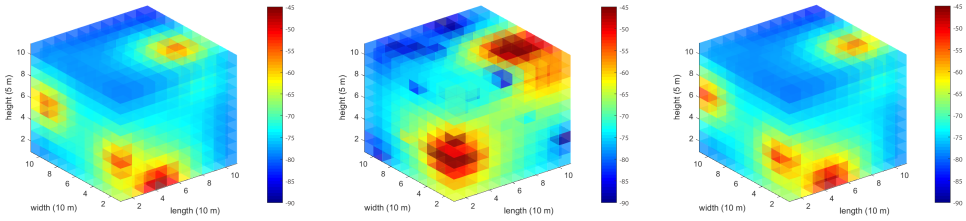


**Figure 5.** Simulation results of 3D ETSM construction: (left) Ideal 3D ETSM; (middle) Original 3D ETSM obtained by random single-UAV; (right) Ultimate 3D ETSM.

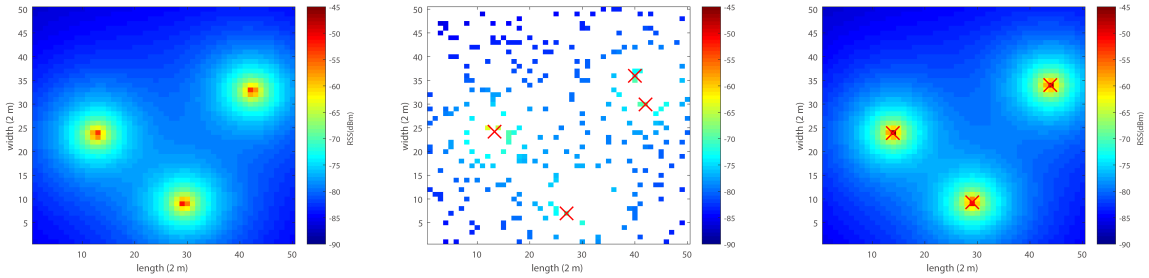


**Figure 6.** Simulation results of target positioning: (left) Ideal 2D plane; (middle) MMPLD-based rough positioning; (right) Ultimate positioning result.

The root mean squared error (RMSE) is introduced to evaluate the accuracy of 3D ETSM construction, as given by

$$RMSE_{\mathrm{ETSM}} = \sqrt{\frac{1}{N}\sum_{n=1}^{N}|P_{\mathrm{est}}(n) - P_{\mathrm{ide}}(n)|}, \tag{20}$$

$$RMSE_{\mathrm{ET}} = \frac{1}{K}\sum_{k=1}^{K}\sqrt{\left\|\phi_k - \widehat{\phi}_k\right\|^2}, \tag{21}$$

where $RMSE_{\mathrm{ETSM}}$ denotes the accuracy of spectrum map recovery, and $P_{\mathrm{est}}$ and $P_{\mathrm{ide}}$ are the estimated and the ideal RSS values in dBm at the $n$-th cube, respectively. $RMSE_{\mathrm{ET}}$ denotes the accuracy of EM target positioning; $K$ is the total number of EM targets; $\phi_k$ and $\widehat{\phi}_k$ are the estimated and the real position of the $k$-th EM target, respectively. $RMSE$s of the result in Figure 4 are listed in Table 2; this highlights that the proposed spectrum data fusion algorithm provides greater performance improvements.

In the simulations, the accuracy of the proposed 3D ETSM construction is compared with IDW, alternating direction method of multipliers (ADMM)[13], and iterative completion method of difference of measurement (ICDM)[32]. Figure 7 (left) shows the RMSEs of spectrum map recovery versus signal-to-noise ratios (SNRs) at 10% sampling rate. The localization performance is also compared with several multi-objective localization methods, including orthogonal matching pursuit (OMP)[33], Bayesian compressed sensing (BCS)[34], and adaptive grid multiple targets localization (AGMTL)[35]. Figure 7 (right) shows the RMSEs of target locations versus SNRs at 10% sampling rate. When the SNR increases from -10 dB to 20 dB, the RMSEs of spectrum map recovery and target location of different methods all decrease. This is because we use the fusion algorithm based on re-weighting, eliminating some outliers generated in the process of spectrum completion.

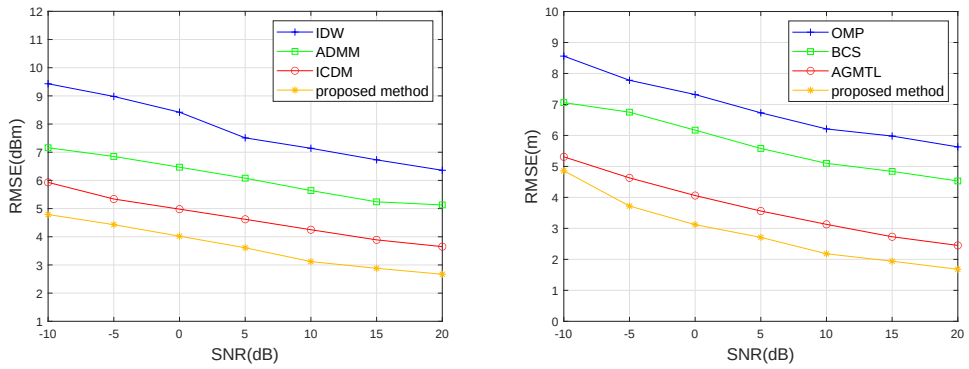


**Figure 7.** (left) The RMSEs of spectrum map recovery of all the methods versus SNRs; and (right) the RMSEs of target locations of all the methods versus SNRs.

**Table 2. RMSEs of 3D ETSM construction**

| Type | $RMSE_{\mathrm{ETSM}}$ (dBm) | Type | $RMSE_{\mathrm{ET}}$(m) |
|---|---|---|---|
| ETSM before fusion | 7.6 | rough positioning | 2.62 |
| ETSM after fusion | 2.24 | ultimate positioning | 1.33 |

## 5. CONCLUSIONS

This paper has proposed a 3D ETSM construction method based on multi-UAV collaboration. Through situational fusion based on re-weighting, complementation of spectrum information has been achieved by multi-UAVs, and the fault tolerance of the ETSM construction system has increased. Furthermore, a staged EM target positioning algorithm based on MMPLD has been proposed for EM target perception. The algorithm rapidly locates multiple EM targets while retaining a certain degree of computing complexity. Compared with existing methods, the simulation results have demonstrated that the proposed 3D ETSM construction method effectively improves the accuracy of spectrum map construction and EM target localization. However, due to the experimental constraints, we only discuss and compare the simulation performance in this paper. In the future research, we will further carry out more field experiments and verify the performance of the proposed construction method.

## DECLARATIONS

### Authors' contributions

Made substantial contributions to conception and design of the study and performed data analysis and interpretation: Peng Y, Liu K, Cai X

Contributed to approach validation, software simulation, and writing-original draft preparation: Peng Y, Wang J

Contributed to the investigation, supervision, and writing-review and preparation: Lin Z

### Availability of data and materials

Not applicable.

### Financial support and sponsorship

This work was supported in part by the National Natural Science Foundation of China under Grant No. 62271250, in part by Natural Science Foundation of Jiangsu Province, No. BK20211182, in part by the Key Technologies R&D Program of Jiangsu (Prospective and Key Technologies for Industry) under Grants BE2022067, BE2022067-1 and BE2022067-3, in part by the States Key Laboratory of Air Traffic Management

System under Grant No. SKLATM202305 and in part by the Shanghai Aerospace Science and Technology Fund under Grant No. SAST2023-023.

### Conflicts of interest

All authors declared that there are no conflicts of interest.

### Ethical approval and consent to participate

Not applicable.

### Consent for publication

Not applicable.

### Copyright



## REFERENCES

1. Ding G, Wu Q, Zhang L, Lin Y, Tsiftsis TA, Yao YD. An amateur drone surveillance system based on the cognitive internet of things. *IEEE Commun Mag* 2018;56:29-35. DOI
2. Huang Y, Zhu X, Wu Q. Intelligent spectrum anti-jamming with cognitive software-defined architecture. *IEEE Syst J* 2023;17:2686-97. DOI
3. Pan J, Ye N, Yu H, et al. AI-driven blind signature classification for IoT connectivity: a deep learning approach. *IEEE Trans Wireless Commun* 2022;21:6033-47. DOI
4. Liu J, Yu J, Niyato D, Zhang R, Gao X, An J. Covert ambient backscatter communications with multi-antenna tag. *IEEE Trans Wireless Commun* 2023;22:6199-212. DOI
5. Höyhtyä M, Mämmelä A, Eskola M, et al. Spectrum occupancy measurements: a survey and use of interference maps. *IEEE Commun Surv Tutorials* 2016;18:2386-414. DOI
6. Phillips C, Ton M, Sicker D, Grunwald D. Practical radio environment mapping with geostatistics. In: 2012 IEEE International Symposium on Dynamic Spectrum Access Networks; 2012. pp. 422-33. DOI
7. Yilmaz HB, Tugcu T, Alagöz F, Bayhan S. Radio environment map as enabler for practical cognitive radio networks. *IEEE Commun Mag* 2013;51:162-9. DOI
8. Du XF, Zhu QM, Wu QH, et al. UAV-assisted spectrum mapping system based on tensor completion scheme. In: MLICOM 2020: Machine Learning and Intelligent Communications; 2021. pp. 16-26. DOI
9. Zhu Q, Zhao Y, Huang Y, et al. DEMO abstract: an UAV-based 3D spectrum real-time mapping system. In: IEEE INFOCOM 2022 - IEEE Conference on Computer Communications Workshops (INFOCOM WKSHPS); 2022. pp. 1-2. DOI
10. Agrawal N, Bansal A, Singh K, Li CP, Mumtaz S. Finite block length analysis of RIS-assisted UAV-based multiuser IoT communication system with non-linear EH. *IEEE Trans Commun* 2022;70:3542-57. DOI
11. Üreten S, Yongaçoğlu A, Petriu E. A comparison of interference cartography generation techniques in cognitive radio networks. In: 2012 IEEE International Conference on Communications (ICC); 2012. pp. 1879-83. DOI
12. Denkovski D, Atanasovski V, Gavrilovska L, Riihijärvi J, Mähönen P. Reliability of a radio environment Map: Case of spatial interpolation techniques. In: 2012 7th International ICST Conference on Cognitive Radio Oriented Wireless Networks and Communications (CROWNCOM); 2012. pp. 248-53. DOI
13. Tang M, Ding G, Wu Q, Xue Z, Tsiftsis TA. A joint tensor completion and prediction scheme for multi-dimensional spectrum map construction. *IEEE Access* 2016;4:8044-52. DOI
14. Hashimoto R, Suto K. SICNN: spatial interpolation with convolutional neural networks for radio environment mapping. In: 2020 International Conference on Artificial Intelligence in Information and Communication (ICAIIC); 2020. pp. 167-70. DOI
15. Yilmaz HB, Tugcu T. Location estimation-based radio environment map construction in fading channels. *Wireless Commun Mob Comput* 2015;15:561-70. DOI
16. Alfattani S, Yongacoglu A. Indirect methods for constructing radio environment map. In: 2018 IEEE Canadian Conference on Electrical & Computer Engineering (CCECE); 2018. pp. 1-5. DOI
17. Wang J, Zhu Q, Lin Z, et al. Sparse bayesian learning-based 3-D radio environment map construction-sampling optimization, scenario-dependent dictionary construction and sparse recovery. *IEEE Trans Cogn Commun Netw* 2023;10:80-93. DOI
18. Zhao Y, Zhu Q, Lin Z, et al. Temporal prediction for spectrum environment maps with moving radiation sources. *IET Commun* 2023;17:538-48. DOI
19. Liu K, Lin Z, Liu Y, Zhu Q, Wu Q, Cai X. A new spectrum map fusing method based on difference group sparsity. In: 2023 IEEE/CIC International Conference on Communications in China (ICCC); 2023. pp. 1-6. DOI
20. Zhang H, Tian Q, Han Y. Multi channel spectrum prediction algorithm based on GCN and LSTM. In: 2022 IEEE 96th Vehicular

Technology Conference (VTC2022-Fall); 2022. pp. 1-5. DOI
21. Zhang H, Peng S, Zhang J, Lin Y. Big data analysis and prediction of electromagnetic spectrum resources: a graph approach. *Sustainability* 2022;15:508. DOI
22. Li S, Sun Y, Zhang H, Wang M, Zhang Z. MTF$^2$N: multi-channel temporal-frequency fusion network for spectrum prediction. In: GLOBECOM 2022 - 2022 IEEE Global Communications Conference; 2022. pp. 4703-9. DOI
23. Cai X, Lin Z, Peng Y, et al. A new variational bayesian-based radiation source positioning method with multistage parameter modification. In: 2023 IEEE/CIC International Conference on Communications in China (ICCC); 2023. pp. 1-6. DOI
24. Trinh-Hoang M, Viberg M, Pesavento M. Partial relaxation approach: an eigenvalue-based DOA estimator framework. *IEEE Trans Signal Proc* 2018;66:6190-203. DOI
25. Zhang Y, Wang M, Tan Z, et al. Design of wireless sensor network location algorithm based on TDOA. In: 2019 IEEE 3rd Information Technology, Networking, Electronic and Automation Control Conference (ITNEC); 2019. pp. 70-75. DOI
26. Liu B, Zhu X, Jiang Y, Wei Z, Huang Y. UAV and piecewise convex approximation assisted localization with unknown path loss exponents. *IEEE Trans Veh Technol* 2019;68:12396-400. DOI
27. Min E, Guo X, Liu Q, Zhang G, Cui J, Long J. A survey of clustering with deep learning: from the perspective of network architecture. *IEEE Access* 2018;6:39501-14. DOI
28. Jordan Y, Carey EP. Semi-supervised K-means++. *arXiv* 2017;87:2597-608. DOI
29. Umer M, Kulik L, Tanin E. Spatial interpolation in wireless sensor networks: localized algorithms for variogram modeling and Kriging. *Geoinformatica* 2010;14:101-34. DOI
30. Bradley E, Trevor H, Iain J, Robert T. Least angle regression. *Ann Stat* 2004;32:407-99. DOI
31. Sun B, Guo Y, Li N, Fang D. Multiple target counting and localization using variational bayesian EM algorithm in wireless sensor networks. *IEEE Trans Commun* 2017;65:2985-98. DOI
32. Lu J, Zha S, Huang J, Liu PG, Chen G, Xu S. The iterative completion method of the spectrum map based on the difference of measurement values. In: 2018 IEEE 3rd International Conference on Signal and Image Processing (ICSIP). IEEE; 2018. pp. 255-59. DOI
33. Tropp JA, Gilbert AC. Signal recovery from random measurements via orthogonal matching pursuit. *IEEE Trans Infor Theory* 2007;53:4655-66. DOI
34. Chi Y, Pezeshki A, Scharf L, Calderbank R. Sensitivity to basis mismatch in compressed sensing. In: 2010 IEEE International Conference on Acoustics, Speech, and Signal Processing; 2010. pp. 3930-33. DOI
35. You K, Yang L, Liu Y, Guo W, Wang W. Adaptive grid multiple sources localization based on sparse bayesian learning. *J Elect Infor Technol* 2018;40:2150-7. DOI